Rare Metal Materials and Engineering
Volume 47, Issue 2, February 2018
Online English edition of the Chinese language journal

Available online at www.sciencedirect.com
ScienceDirect

Cite this article as: Rare Metal Materials and Engineering, 2018, 47(2): 0409-0415.

ARTICLE

Hot Deformation Behavior and Processing Maps of AA7085 Aluminum Alloy

Yang Qunying[1], Liu Wenyi[2], Zhang Zhiqing[1], Huang Guangjie[1], Liu Xiaoyong[1]

[1] Chongqing University, Chongqing 400044, China; [2] Shaanxi University of Technology, Hanzhong 723003, China

Abstract: The flow behavior and processing maps of homogenized AA7085 aluminum alloy were investigated by isothermal hot compression tests in the temperature range of 300~450 °C with strain rates of 0.01~10 s^{-1}. Microstructure was characterized using Optical microscopy (OM), electron back-scattered diffraction (EBSD) and transmission electron microscopy (TEM). The results show that the superimposed processing maps at different strains exhibit the optimized deformation parameters with the temperature of 390~450 °C and strain rates lower than 0.1 s^{-1}. Microstructure characterization reveals that dynamic recovery and recrystallization are the main deformation mechanisms in the safe regions. At lower temperature and lower strain rate, the coarsening of particles between ε=0.5 and ε=0.7 may be responsible for the transformation of processing map from unstability to safe domain.

Key words: 7085 aluminum alloy; flow behavior; processing maps; flow localization; optimum parameter

AA7085 aluminum alloy belonging to 7000 (Al-Zn-Mg-Cu) series alloys was firstly introduced by ALCOA in 2003 as the 7th generation of high strength thick plate alloy[1-3]. Because of its high strength to low densities and high fracture toughness, as well as resistance to stress corrosion cracking, it is widely used for aerospace applications, such as wing spar and rib structures on the new Airbus A380 airliner[1].

Workability of metal can be evaluated by means of processing map, which developed from flow stress variation related to strain, strain rate, and temperature. In the past several decades, extensive researches focused on high temperature plastic deformation behavior and processing maps of 7000 series aluminum alloys have determined the optimum fabrication conditions[4-7]. Processing maps have been proven to be a useful tool for optimizing the hot working parameters. However, more and more attention was put on the processing maps based on the special strain, which were used to predict material processing parameters[8,4,9]. Less works have been done on the evolution of processing maps at different strains during hot deformation, while recent researches have pointed out that strain plays a very important role in the processing map evolution. The change of strain can accelerate the transformation from unsafe domain to safe domain in Al-Si-Mg alloys and 7A09 aluminum alloy[10,7]. However, detailed study of microstructure characteristics at different strain levels and restoration mechanism during deformation are rarely reported.

In the present study, a superimposed processing map at different strains was used to determine the optimum condition. Microstructure evolution and softening mechanism are investigated by a detailed microstructure characterization at different strain levels. The aim is to obtain optimum parameter and better understand restoration mechanism of AA7085 aluminum alloy for thermo-mechanical processing, which provides a guide to optimize industrial hot deformation schedules.

1 Experiment

The chemical composition (wt%) of the AA7085 aluminum alloy in this work was as follows: 7.6Zn, 1.5Mg, 1.8Cu, 0.08Zr, Fe≤0.08, and Si≤0.06. The cast ingot were

Received date: February 14, 2017
Foundation item: the International Science & Technology Cooperation Program of China (2014DFA51270); the Fundamental Research Funds for the Central Universities (CDJRC10130008, 106112015CDJXZ138803, 106112015CDJXY130003); National Natural Science Foundation of China (51421001)
Corresponding author: Zhang Zhiqing, Ph. D., Professor, College of Material Science and Engineering, Chongqing University, Chongqing 400044, P. R. China, Tel: 0086-23-65103045, E-mail: zqzhang@cqu.edu.cn

homogenized at 400 °C for 12 h and 460 °C for 12 h, and then rapidly quenched into room-temperature water.

The specimens were cut from the ingot with dimension of Φ10 mm×15 mm. The isothermal compression tests were carried out on a computer servo-controlled Gleeble-3500 simulator in the temperatures range from 300 to 450 °C, at the strain rates of 0.01, 0.1, 1, 10 s^{-1}. The cylindrical compression specimens were heated to deformation temperature with heating rate of 5 °C/s and held for 3 min prior to compression. The specimens were deformed to the total true strain of ε = 0.9 and the required strain level. After compression, the samples were quenched to room temperature immediately to maintain deformation microstructure.

The deformed samples were sectioned parallel to the compression axis along the direction of centerline. Microstructure was analyzed using optical microscopy (OM), electron backscatter diffraction (EBSD) and transmission electron microscopy (TEM). The preparation of OM and EBSD specimens was electro-polished in a 10% $HClO_4$ and 90% C_2H_5OH solution with current density of 1.5 A·cm^{-2} for 30 s at –20 °C. The EBSD test was conducted using a field emission gun-environmental scanning electron microscopy (FEG-SEM) FEI device equipped with an HKL Channel 5 EBSD System. The TEM sample was a 50~60 μm foil and then twin-jet polished in a 30% HNO_3 and 70%CH_4O solution. TEM examination was performed using a FEI TECNAL G2 F20 TEM microscope operated at 200 kV.

2 Results and Discussion

2.1 True stress-true strain curves

True stress-true strain curves obtained from 300 °C to 450 °C with various strain rates are shown in Fig.1. It can be seen that the flow stress increases with increasing the strain rate or decreasing the temperature. In addition, the flow stress after the peak strain reaches a stable state at low strain rates ($\dot{\varepsilon} \leqslant 1$ s^{-1}), indicating the balance between the work hardening and dynamic softening. At high strain rates ($\dot{\varepsilon} \geqslant 10$ s^{-1}), the flow curves after the peak strain decrease monotonically till the final strain and a continuous softening are obtained. According to the study of R. Bhattacharya and Byoung Ho Lee [11,12], deformation heating becomes prominent at high strain rate ($\dot{\varepsilon} \geqslant 1$ s^{-1}), resulting in a thermal softening in materials. Combined with the results of set-temperatures and the actual temperatures (Fig.2a~2d), the actual temperatures have significant difference compared to the set-temperature at high strain rates ($\dot{\varepsilon} \geqslant 1$ s^{-1}). The increment of temperature reaches to ~35 °C compared to the pre-set temperature at strain rate of 10 s^{-1}. Therefore, the flow stress corrected (σ^1) for deformation heating is necessary and it can be defined as follows[13]:

$$\sigma^1(\varepsilon,\dot{\varepsilon},T_0) = \sigma^H(\varepsilon,\dot{\varepsilon},T_0) - \frac{\partial\sigma^1(T_0)}{\partial(T_0)}\Big|_{(\varepsilon,\dot{\varepsilon})}\Delta T \quad (1)$$

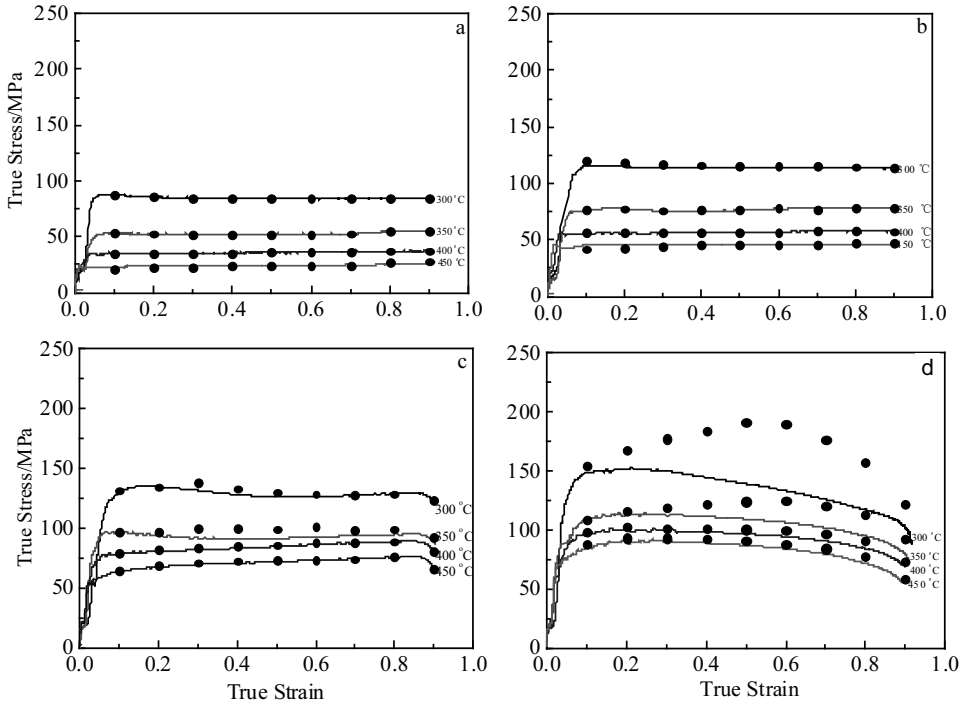

Fig. 1 True stress-true strain curves of AA7085 aluminum alloy deformed with different strain rates: (a) 0.01 s^{-1}, (b) 0.1 s^{-1}, (c) 1 s^{-1}, and (d) 10 s^{-1}

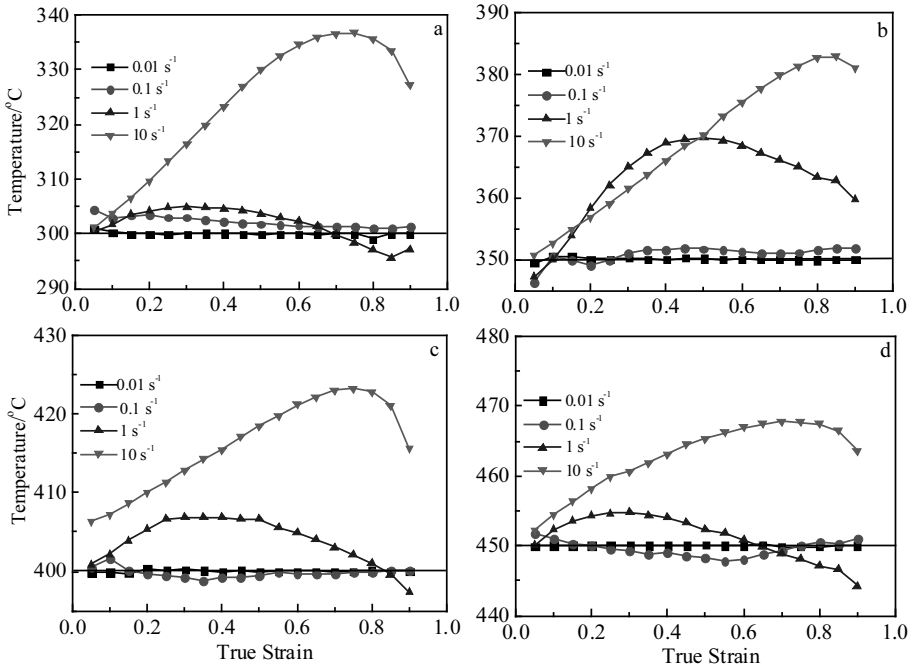

Fig.2 Actual temperatures of AA7085 aluminum alloy during isothermal compression at different set temperatures: (a) 300 °C, (b) 350 °C, (c) 400 °C, and (d) 450 °C

where σ^{H} is the flow stress uncorrected for deformation heating, and T_0 is the initial test temperature. The corrected flow stress marked with the black dots is shown in Fig.1. It is noted that the corrected flow stress at lower strain rate does not exhibit obvious difference, while it becomes remarkable at high strain rate. Thus, deformation heating is one of reasons to affect the flow stress.

2.2 Processing maps

Processing maps based on the dynamic materials models (DMM) theory were established [14-16]. The efficiency of power dissipation, η, which is a function of temperature and strain rate, defined as follows:

$$\eta = \frac{2m}{m+1} \tag{2}$$

where m represents the strain rate sensitivity. The variation of the efficiency of power dissipation indicates microstructure changes, which can be described by iso-efficiency contour map. However, the value of power dissipation may be high in the instability domains and can not describe the processability. Based on the principle of the maximum rate of entropy production, the flow instability parameter $\xi(\dot{\varepsilon})$ is given as:

$$\xi(\dot{\varepsilon}) = \frac{\partial \ln[m/(m+1)]}{\partial \ln \dot{\varepsilon}} + m \le 0 \tag{3}$$

The variation of the instability parameter represents an instability map, which is described by the gray region. Therefore, processing maps can be obtained by superimposing the instability map over the power dissipation map.

The processing maps of AA7085 aluminum alloy at various strains for uncorrected flow stress are presented in Fig.3. It can be seen that the flow instability regions and safe areas have no obvious change at low strains ($\varepsilon \leqslant 0.5$), as shown in Fig.3a and Fig.3b. With the increasing strain, the former unstable region Ⅰ is transformed into a new safe domain at a strain of $\varepsilon = 0.7$ (300~360 °C, 0.01~0.1 s^{-1}), as marked with Ⅰ in Fig.3c. The power dissipation efficiency have no obvious difference between $\varepsilon = 0.3$ and $\varepsilon = 0.5$, while it increases from 0.25 to 0.68 with increasing strain from $\varepsilon = 0.5$ to $\varepsilon = 0.7$. However, safe area Ⅱ diminishes gradually as the deformation proceeds. A combined processing map by a superposition of processing maps at strains of $\varepsilon = 0.3$, $\varepsilon = 0.5$ and $\varepsilon = 0.7$ is shown in Fig.3d. The safe domain Ⅳ is the intersection of all the safe deformation areas in the three processing maps. The deformation parameters of the temperature range of 390~450 °C and strain rates lower than 0.1 s^{-1} are determined for optimum processing, where the highest efficiency of power dissipation is 0.45. The efficiency of power dissipation indicates the workability of material. The higher the power dissipation, the easier the process. Thus, the safe domain Ⅳ is determined for optimum processing. It is noticed that the safe domain in the processing maps at the certain strain may not be reliable for optimizing working parameters. Therefore, a superposition of the processing maps at different strains is necessary.

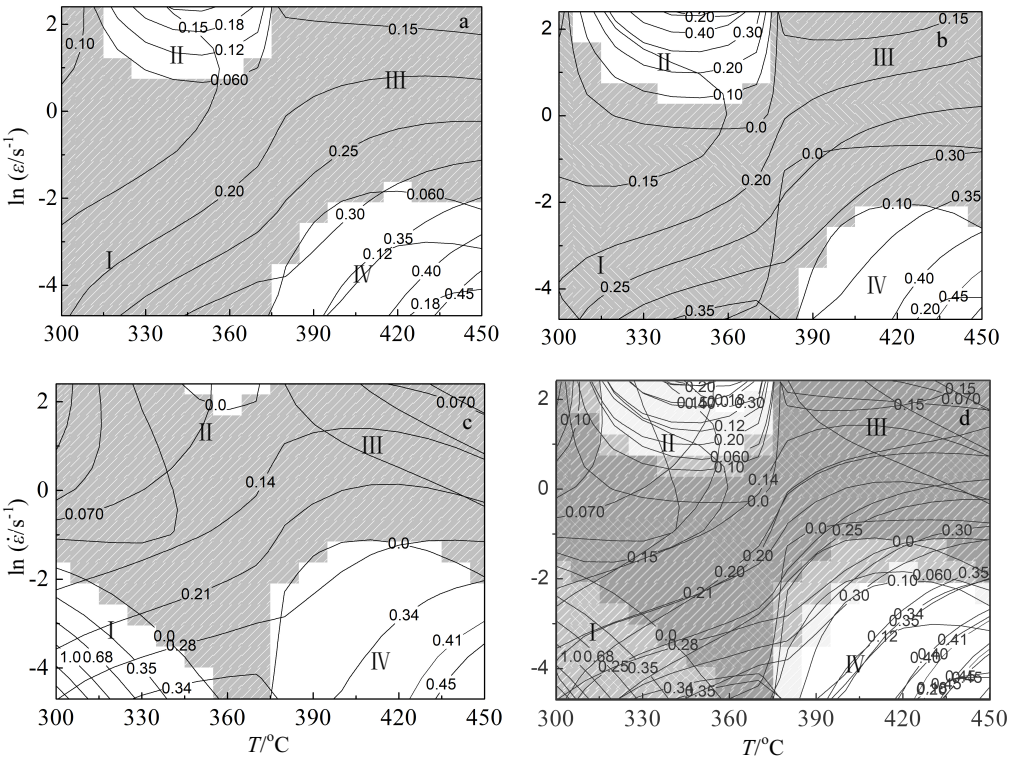

Fig.3 Processing maps of uncorrected flow stress for deformation heating: (a) $\varepsilon=0.3$, (b) $\varepsilon=0.5$, (c) $\varepsilon=0.7$ and (d) the superposition process maps at various strains

2.3 Microstructure examination

The corresponding microstructures compressed to a total strain of $\varepsilon=0.9$ under the different conditions as indicated by letters in Fig.2 (from Ⅰ~Ⅳ) are shown in Fig.4. It can be seen that the microstructures in the instability regions consist of elongated grains and flow locations marked with white arrows, indicating the occurrence of flow instability (Fig.4a, 4b). It may be ascribed to the deformation heating. At high strain rates ($\geqslant 1$ s^{-1}), energy due to deformation heating cannot be removed from the specimens, leading to an increase in actual temperature and the occurrence of local flow instability in special grains. As the strain rate decreases, the microstructure of 350 °C, 0. 01 s^{-1} specimen exhibits prominently the dynamic recovery (Fig.4c), while the microstructure of 450 °C, 0.01 s^{-1} specimen reveal that new equiaxed grains spread along grain boundaries, illustrating that main softening mechanism is recovery and recrystallization (Fig.4d). However, the processing map evolutions of the corresponding Ⅰ and Ⅳ regions exhibit obvious difference. Therefore, a study of microstructure evolution of AA7085 aluminum alloy deformed at 350 °C, 0.01 s^{-1} and 450 °C, 0.01 s^{-1} with various strain levels are necessary to reveal the control mechanism of different deformation parameters in the present study.

In order to reveal the transformation from unsafe domain to safe domain at the bottom left of the processing maps, the microstructure evolution of the 350 °C, 0.01 s^{-1} deformed specimens were studied by electron backscatter diffraction (EBSD) technique, as shown in Fig.5. In these corresponding EBSD maps, boundaries with further misorientations of 2°~5°, 5°~10°, 10°~15° and > 15° are described by green lines, red lines, blue lines and black lines, respectively. At a strain of ε=0.3, grains have no remarkable changes compared to the initial microstructure (Fig.5a). With the increasing strain, original grains are elongated and the majority of low-angle grain boundaries accumulate preferentially along grain boundaries (Fig.5b). As the strain increases to $\varepsilon=0.7$ (Fig.5c), low-angle grain boundaries gradually extend toward the grain centre and across the whole deformed grains, leading to the formation of recovery structure. By further straining to $\varepsilon=0.9$, more and more sub-boundaries are formed within grains and some isolated high-angle grain boundary segments marked with white arrows are observed (Fig.5d), suggesting that the transformation from low-angle grain boundaries to high-angle grain boundaries is found and dynamic recovery is the dominant softening mechanism. It is noted that microstructure characterization of EBSD does not agree with the transformation of the processing maps between $\varepsilon=$

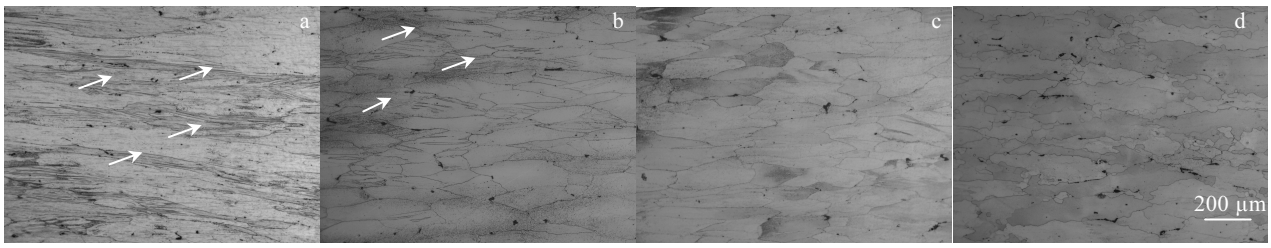

Fig.4 Microstructures of the deformed specimens compressed under different conditions: (a) 350 °C, 10 s^{-1}; (b) 400 °C, 10 s^{-1}; (c) 350 °C, 0.01 s^{-1}; (d) 450 °C, 0.01 s^{-1}

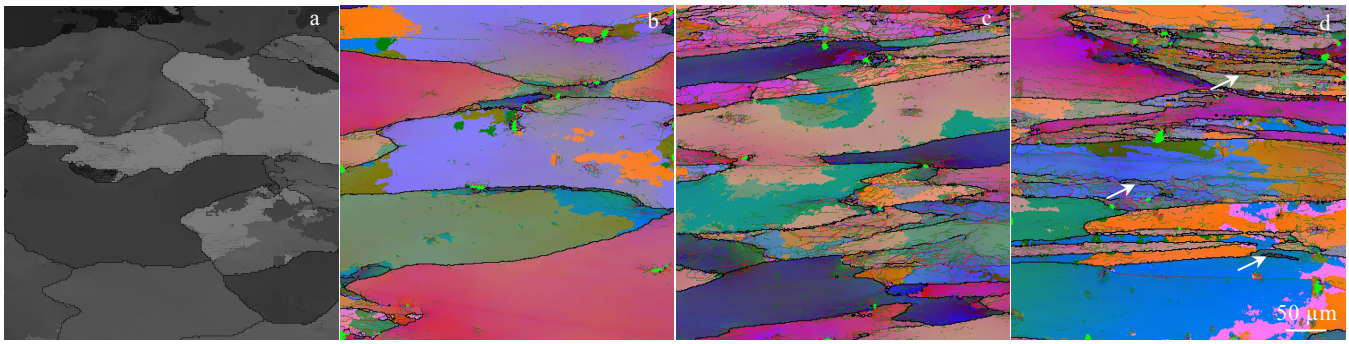

Fig.5 EBSD images of AA7085 aluminum alloy deformed with various strains at 350 °C, 0.01 s^{-1}: (a) $\varepsilon=0.3$, (b) $\varepsilon=0.5$, (c) $\varepsilon=0.7$, and (d) $\varepsilon=0.9$

0.3 and $\varepsilon=0.7$. Previous studies have pointed out the typical microstructural manifestations in the unsafe domain are related to adiabatic shear bands, flow localizations, pore, kink bands, deformation bands[17-19,10,4]. These instable microstructures may be responsible for the change of processing maps. However, the present study seems to disagree with the previous studies.

The corresponding TEM micrographs of the 350 °C, 0.01 s^{-1} specimens compressed to various strains are shown in Fig.6. At a strain of ε=0.3, high density of dislocations accompanied with fine particles with mean size of 50 nm are presented within deformed grains (Fig.6a). With increasing strain from $\varepsilon=0.3$ to $\varepsilon=0.5$, more fine particles precipitate from matrix and the number density of particles increases from 2.2×10 to 4.2×10^7 mm^{-2}, while the average size of particles in both specimens has no significant change (Fig.6b). By further straining to $\varepsilon = 0.7$, cell-dislocation structure evolves into sub-grains and the average size of particles with the number density of 4.3×10^7 mm^{-2} is about 65 nm (Fig.6c), indicating that precipitate coarsening becomes prevalent when deformation is continued to $\varepsilon = 0.7$. As the strain increases to $\varepsilon = 0.9$ (Fig.6d), sub-grains coarsening are found due to the sub-grain growth. Such a microstructure evolution suggests that recovery accompanied with dynamic precipitation and coarsening is the main softening mechanism.

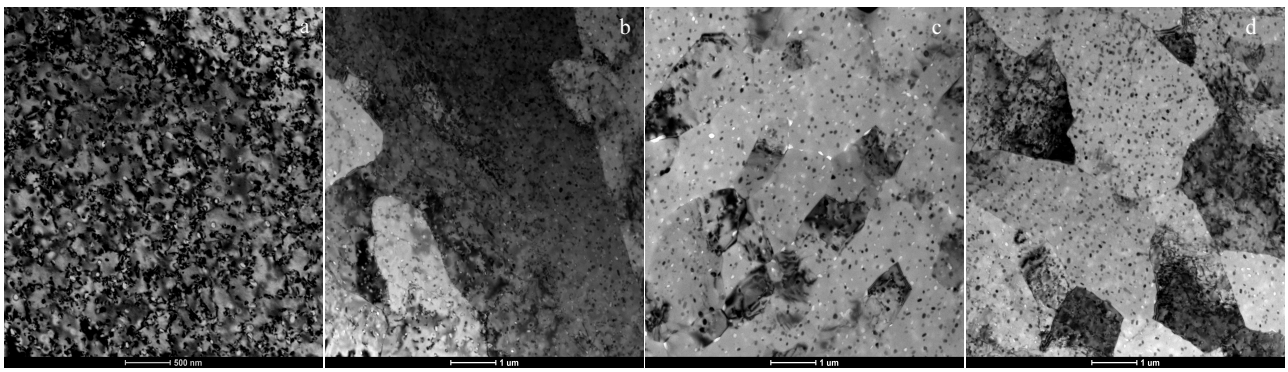

Fig.6 TEM micrographs of the specimens deformed with different strains at 350 °C, 0.01 s^{-1}: (a) $\varepsilon=0.3$, (b) $\varepsilon=0.5$, (c) $\varepsilon=0.7$, and (d) $\varepsilon=0.9$

In combination with the all Euler images and TEM micrographs of the specimens subjected to various strains, it is confirmed that the occurrence of instability is related to the dynamic precipitation and coarsening. Due to high solution level during homogenization, the majority of alloying elements are reserved in the matrix in the form of solutes. After low temperature deformation, small particles with various shapes are precipitated due to low super-saturation, which is called strain-induced precipitation[20]. These fine particles can inhibit dislocation mobility, leading to an increase in the fraction of low-angle grain boundary. Moreover, as the deformation proceeds, the coarsening of particles increases the spacing of precipitate and facilitates the formation of subgrain [21]. Consequently, well-developed sub-grains are formed at high strains ($\varepsilon \geqslant 0.7$), indicating that recovery can retard recrystallization. The combining effects of recovery, dynamic precipitation and coarsening on the efficiency of power dissipation lead to a significant change in the processing maps. The coarsening of particles between $\varepsilon = 0.5$ and $\varepsilon = 0.7$ may be responsible for the transformation from unstability to safe domain as marked with letter Ⅰ. Therefore, the processing map is only a reference factor to indicate hot workability of materials and can not be used to judge safety under this condition.

According to the superimposed processing maps (Fig.3d), the stability regions occur in the temperature range of 390 ~450 °C with strain rates of 0.01 ~ 0.1 s^{-1}. The maximum power dissipation efficiency of 45% is observed at 450 °C and 0.01 s^{-1}, indicating the good workability. Thus, the microstructure evolution process of materials at 450 °C, 0.01 s^{-1} is displayed in Fig.7. It can be seen that new recrystallized grains marked with arrows are observed at triple junctions and grain boundaries after straining to $\varepsilon =$ 0.3 and $\varepsilon = 0.5$ (Fig.7a and Fig.7b), indicating that the dynamic recrystallization occurs preferentially at triple junctions and original boundaries. With increasing strain, fine recrystallized grains spread along grain boundaries and more sub-grains are developed in coarse grain interiors (Fig.7c, 7d). The microstructure consists of elongated grains and fine grains, indicating the occurrence of typical partial DRX at 450 °C, 0.01 s^{-1}.

By comparison of Fig. 6a to 6d, another difference in the TEM micrographs becomes more evident (Fig.8). The second-phase particles have been dissolved at 450 °C and the contribution of particles to the efficiency of power dissipation can be weakened during deformation process. TEM micrographs reveal that original grains are fragmented progressively by low-angle boundaries and high density dislocation walls (Fig.8a-8b), illustrating the occurrence of remarkable recovery. As the strain increases,

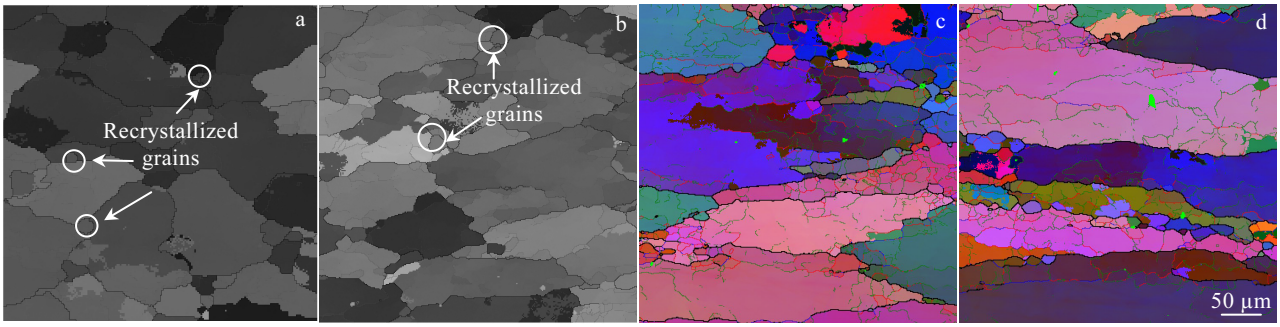

Fig.7 EBSD images of AA7085 aluminum alloy deformed with different strains at 450 °C, 0.01 s^{-1}: (a) $\varepsilon = 0.3$, (b) $\varepsilon = 0.5$, (c) $\varepsilon = 0.7$, and (d) $\varepsilon = 0.9$

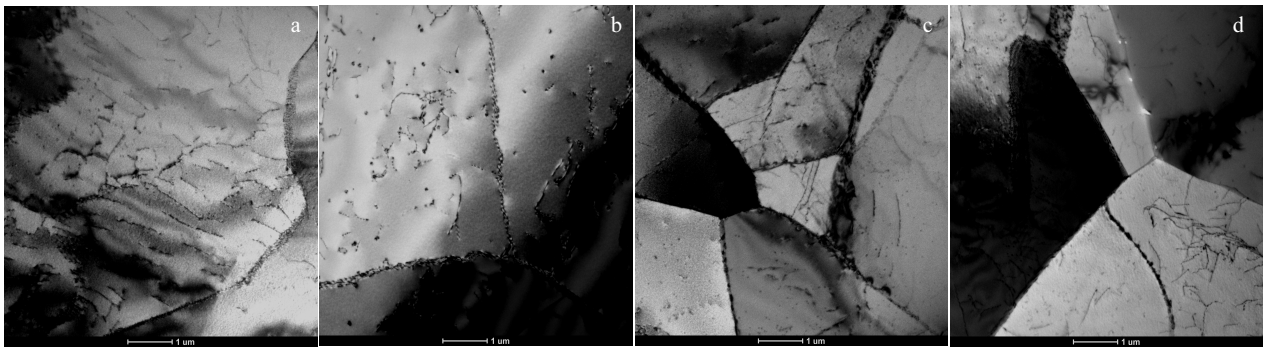

Fig.8 TEM micrographs of the specimens deformed with different strains at 450 °C, 0.01 s^{-1}: (a) $\varepsilon = 0.3$, (b) $\varepsilon = 0.5$, (c) $\varepsilon = 0.7$, and (d) $\varepsilon = 0.9$

the complex rearrangement and annihilation of dislocation lead to the formation of straight and clear boundaries (Fig.8c, 8d), illustrating that the recovery is extended and the dynamic recrystallization occurs. Such a microstructure evolution exhibits the feature of dynamic recovery and recrystallization. Therefore, dynamic recovery and recrystallization does not result in the obvious change of the efficiency of power dissipation in domain Ⅳ during deformation process. As a consequence, the processing maps in domain Ⅳ is still in the state of safe.

3 Conclusions

1) The flow behavior is affected by strain rate and temperature. Continuous flow softening behavior is prone to occur at high strain rates ($\dot{\varepsilon} \geqslant 10\ s^{-1}$), indicating that the occurrence of flow instability during isothermal compression is ascribed to deformation heating.

2) A superimposed processing map at different strains is proposed. The optimum parameters are determined in the deformation temperature range of 390 ~450 °C and strain rates of 0.01~0.1 s^{-1}. Dynamic recovery and recrystallization are main softening mechanism in the safe domain.

3) Without considering the deformation heating, the transformation of processing map from the instability region to the safe region may be related to the coarsening of particles.

References

1 Harold Luong, Michael R H. *Materials Science and Engineering A*[J], 2008, 477: 208

2 He Lizi, Li Xiehua, Zhu Pei *et al*. *Materials Characterization* [J], 2012, 71: 19

3 Chen Songyi, Chen Kanghua, Peng Guosheng *et al. Materials and Design*[J], 2012, 35: 93

4 Yang Yongbiao, Zhang Zhimin, Li Xubin *et al. Materials and Design*[J], 2013(5): 592

5 Lin Y C, Li L T, Xia Y C *et al. Journal of Alloys and Compounds*[J], 2013, 550: 438

6 Rajamuthamilselvan M, Ramanathan S. *Journal of Alloys and Compounds*[J], 2011, 509: 948

7 Luo J, Li M Q, Ma D W. *Materials Science and Engineering A* [J], 2012, 532: 548

8 Zhang Tian, Tao Yourui, Wang Xueyin. *Transactions of Nonferrous Metals Society of China*[J], 2014, 24: 1337

9 Ma Xiong, Zeng Weidong, Tian Fei *et al. Materials Science and Engineering A*[J], 2012, 545: 132

10 Liao Hengcheng, Wu Yuna, Zhou Kexin *et al. Materials and Design*[J], 2015, 65: 1091

11 Bhattacharya R, Wynne B P, Rainforth W M. *Scripta Materialia*[J], 2012, 67: 277

12 Lee Byoung Ho, Reddy N S, Yeom Jong Taek *et al. Journal of Materials Processing Technology*[J], 2007, 187-188: 766

13 Zhang Jingqi, Di Hongshuang, Wang Xiaoyu *et al. Materials and Design*[J], 2013, 44: 354

14 Prasad Y V R K, Gegel H L, Doraivelu S M *et al. Metallurgical and Materials Transactions A*[J], 1984, 15: 1883

15 Prasad Y V R K, Seshacharyulu T. *International Materials Reviews*[J], 1998, 43: 243

16 Prasad Y V R K, Rao K P. *Materials Science and Engineering A* [J], 2005, 391: 141

17 Cheng Liang, Xue Xiangyi, Tang Bin *et al. Materials Science and Engineering A*[J], 2014, 606: 24

18 Reddy G J, Srinivasan N, Gokhale A A *et al. Journal of Materials Processing Technology*[J], 2009, 209: 5964

19 Yan J, Pan Q L, Li B *et al. Journal of Alloys and Compounds*[J], 2015, 632: 549

20 Lang Yujing, Cai Yuanhua, Li Huacui *et al. Materials and Design*[J], 2011, 32: 4241

21 Sepehrband P, Wang X, Jinc H *et al. Acta Materialia*[J], 2015, 94: 111

AA7085 铝合金热变形行为及加工图的研究

杨群英[1]，刘文义[2]，张志清[1]，黄光杰[1]，刘晓勇[1]

(1. 重庆大学，重庆 400044)

(2. 陕西理工大学，陕西 汉中 723003)

摘　要：采用等温热压缩试验，研究了AA7085铝合金在变形温度为300～450 ℃、应变速率为0.01～10 s^{-1}的条件下的热变形行为和加工图。通过光学显微镜（OM），电子背散射（EBSD）和透射电镜（TEM）表征了材料的微观组织。结果表明在不同应变条件下的加工图的叠加得到优化的工艺参数为：温度为390~450 ℃，应变速率低于 0.1 s^{-1}. 微观组织表征表明了在安全区内，动态回复和动态再结晶是主要的变形机制。而在低温低速的条件下，在应变0.5与0.7之间的第二相粒子的粗化可能是导致加工图从失稳区向安全区转换的原因。

关键词：7085 铝合金；流变行为；加工图；微观组织；参数优化

作者简介：杨群英，女，1983 年生，博士，重庆大学材料科学与工程学院，重庆 400044，E-mail: 412829912@qq.com